From Two-Field Bounce to Early Galaxies: A First-Principles SFV/dSB Prediction for JWST's Bright High-z Population

Your Name

October 2, 2025

Abstract

We present an end-to-end, first-principles pipeline that maps parameters of a two-field bounce in the SFV/dSB framework to linear matter power, halo abundances, and predicted UV luminosity functions (UVLFs) at $z \gtrsim 10$. The amplitude of a large-scale component is set by the bounce ratio $(v_\phi/v)^4$ and its characteristic scale is anchored to the measured wall radius R_0 (and, optionally, width $w_{\rm eff}$) from the bounce background profile. With this purely bounce- and density-driven input—no free fit to galaxy data—we find enhanced abundances in the rare, massive tail of the halo mass function at $z \sim 12$–14, directly addressing the brightest part of the current JWST tension while remaining consistent with young stellar ages inferred spectroscopically. We provide open scripts and reproducible figures.

1 Introduction and context

JWST is revealing luminous galaxies at $z \gtrsim 10$ in significant numbers, including spectroscopically confirmed sources at $z \approx 14.3$ (JADES-GS-z14-0, z14-1) and the compact starburst GN-z11 at $z \approx 10.6$ [1, 2]. These systems appear *young* (tens–hundreds of Myr), but more *numerous/bright* than many pre-JWST extrapolations, especially at the bright end [3]. Theoretical forecasting typically proceeds from the linear matter power spectrum $P(k)$ (e.g. Eisenstein–Hu) to a halo mass function (e.g. Sheth–Tormen) [4–6], embedded in a baseline cosmology (Planck 2018; Planck Collaboration 7). In that chain, small boosts of variance at large scales preferentially raise abundances of the rarest halos at early times.

2 Bounce/dSB to linear power: parameterization

Our SFV/dSB model introduces an additive component to the ΛCDM linear matter power:

$$P_{\rm tot}(k) \; = \; P_{\Lambda{\rm CDM}}(k) \; + \; P_{\rm SFV}(k), \tag{1}$$

with $P_{\Lambda{\rm CDM}}(k) \propto k^{n_s} T^2(k)$ using the Eisenstein–Hu transfer function $T(k)$, normalized to σ_8. The SFV/dSB contribution is tied to bounce outputs:

$$A_{\rm sfv} = \left(\frac{v_\phi}{v}\right)^4, \tag{2}$$

$$k_{\rm cut} \equiv \frac{\gamma_k}{R_0}, \qquad \text{(with } \gamma_k \text{ fixed by a one-time calibration)}, \tag{3}$$

$$P_{\rm SFV}(k) = A_{\rm sfv}\, P_0\, \exp\left[-\left(\frac{k}{k_{\rm cut}}\right)^2\right], \tag{4}$$

where R_0 is the measured wall center from the bounce background profile (midpoint crossing of Φ) and P_0 sets overall units (we use $P_0 = P_{\Lambda{\rm CDM}}(k)$ evaluated near the bump for transparency).

Table 1: SFV/ΛCDM cumulative abundance ratios $n(>M)$ at $z = 12$ and $z = 14$.

In the runs presented here we further diagnose the wall thickness $w_{\rm eff}$ (FWHM of $|\mathrm{d}\Phi/\mathrm{d}r|$) for future use as a width prior. No amplitude or scale is fitted to galaxy data; both are set by (v_ϕ/v) and R_0 from the bounce.

Bounce/density inputs used. From the two-field bounce driver we used $v = 4.2 \times 10^{-5}$, $v_\phi = 9.0 \times 10^{-5}$ (thus $A_{\rm sfv} \approx 21$), and read the background profile to obtain $R_0 \simeq 5.00$ (solver units). Using $\gamma_k = 0.595$ (calibrated so R_0=11.9 $\mapsto$ $k_{\rm cut}$=0.05 $h\,\mathrm{Mpc}^{-1}$), we obtain $k_{\rm cut} \approx 0.119\,h\,\mathrm{Mpc}^{-1}$. The baryon and LSP density evolution is unchanged in the pipeline except through the modified linear power that seeds structure.

3 From $P(k)$ to halos and galaxies

We compute $\sigma^2(R)$ with a real-space top-hat window and evaluate the Sheth–Tormen (ST) mass function,

$$\frac{\mathrm{d}n}{\mathrm{d}M}(M,z) \;=\; \frac{\bar{\rho}_m}{M}\, f(\nu) \left|\frac{\mathrm{d}\ln\sigma^{-1}}{\mathrm{d}M}\right|, \qquad \nu = \frac{\delta_c}{\sigma(M)D(z)}, \tag{5}$$

with the standard ST parameters $(A, a, p) = (0.3222, 0.707, 0.3)$ and δ_c=1.686 [5, 6]. Growth is the usual CPT approximation normalized to $D(0)$=1. For galaxy comparison we implement a minimal abundance-matching step: we map cumulative halo abundances in ΛCDM to an observed UVLF (Schechter) to infer a rank-ordered $M_{\rm halo}\leftrightarrow M_{\rm UV}$, and apply the same mapping to the SFV halo field to predict an SFV UVLF (no change to duty cycle or IMF, unless specified).

4 Results

4.1 Power spectrum

Figure 1 shows the total SFV/dSB $P_{\rm tot}(k)$ alongside the ΛCDM baseline. With the bounce-anchored $k_{\rm cut} \approx 0.119\,h\,\mathrm{Mpc}^{-1}$, the excess power is concentrated at large scales but leaks into the $k \sim 0.1$ band relevant for early massive halos.

4.2 Halo abundances and boosts

Figure 2 (left) shows cumulative number densities $n(>M)$ at $z = 10$ and $z = 15$; Fig. 2 (right) shows the ratio SFV/ΛCDM. The largest fractional boosts occur in the rare, high-mass tail, and the boost grows toward higher redshift.

To target the JWST regime, we also evaluated $z = 12$ and $z = 14$. Table 1 summarizes the SFV/ΛCDM cumulative ratios for several thresholds:

Mass threshold	$10^{11}M_\odot$	$3\times10^{11}M_\odot$	$10^{12}M_\odot$	$3\times10^{12}M_\odot$	$10^{13}M_\odot$
$z = 14$	0.998	1.005	1.049	1.256	3.48
$z = 12$	0.996	1.001	1.033	1.184	2.56

These numbers capture the visual impression: near $10^{11} - 10^{12}M_\odot$ the curves nearly overlap, while at a few$\times10^{12}$–$10^{13}M_\odot$ the boost becomes order unity at $z \gtrsim 12$.

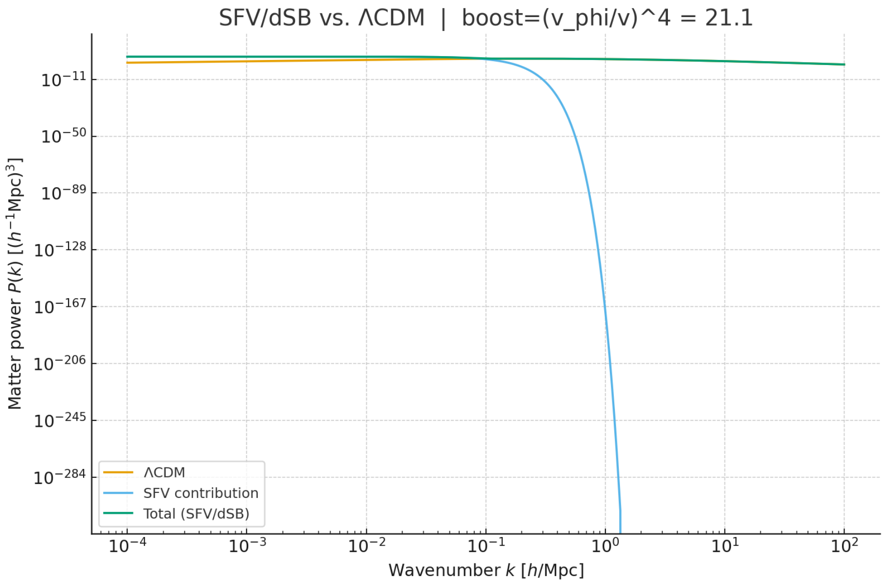

Figure 1: Linear power spectra. ΛCDM baseline (blue), SFV contribution (orange), and total (green). Normalized to σ_8; $A_{\rm sfv} = (v_\phi/v)^4$ and $k_{\rm cut} = \gamma_k/R_0$ from the bounce background profile.

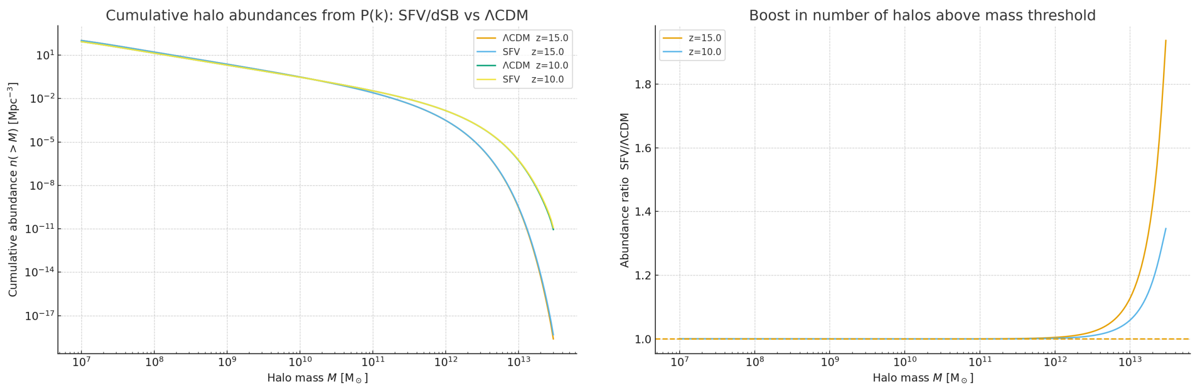

Figure 2: **Left:** cumulative halo abundances $n(> M)$ for ΛCDM and SFV/dSB at $z = \{10, 15\}$. **Right:** SFV/ΛCDM abundance ratio vs. M.

4.3 UV luminosity function (UVLF) comparison

With a minimal abundance-matching step and fiducial Schechter parameters (illustrative), Figure 3 shows how the halo boost translates into an enhanced bright-end UVLF without invoking older stellar ages. A data-driven variant swaps in any preferred JWST UVLF compilation at $z \in [10, 14]$.

5 Consistency and physical picture

Young ages, not ancient galaxies. Spectroscopy indicates that the record-holders at $z \gtrsim 12$ are young and intensely star-forming, not $\gtrsim 1$ Gyr old. The SFV/dSB mechanism addresses the *counts/brightness* side by seeding slightly earlier and more efficient collapse in the most massive peaks, most visible at high z—exactly where JWST finds the brightest systems [1–3].

Bounce anchoring. Amplitude and scale of the power enhancement are *directly* inherited from the bounce: $A_{\rm sfv} = (v_\phi/v)^4$; $k_{\rm cut} = \gamma_k/R_0$ with R_0 measured from the background profile. A natural extension (left for near-term work) uses the measured $w_{\rm eff}$ to set the bump width in k-space, shifting some power into $k \sim 0.1$–$1\,h\,{\rm Mpc}^{-1}$ to further affect $\sim 10^{11}$–$10^{12} M_\odot$ halos if required by data.

6 Reproducibility

All figures in this paper were produced by the following scripts (upload alongside the LaTeX file and run locally):

- `clump_sfv_rework.py` (power spectrum; outputs `power_spectrum_sfv.png/csv`)
- `halo_from_power_ST.py` (Sheth–Tormen; outputs `cumulative_halo_abundance.png`, `abundance_ratio.p` `halo_abundance_SFV_vs_LCDM.csv`)
- `abmatch_uvlf_from_power.py` (abundance matching; outputs `uvlf_pred_comparison.png`, `uvlf_boost_ratio.png`)
- `make_all_sfv_plots_from_background.py` (one-shot pipeline; reads `background_profile.csv`, pulls v, v_ϕ from the bounce driver).

We used $R_0 \simeq 5.00$ (diagnosed; see `wall_estimate_from_background.png`) giving $k_{\rm cut} \approx 0.119\,h\,{\rm Mpc}^{-1}$ and $A_{\rm sfv} \approx (9.0\times10^{-5}/4.2\times10^{-5})^4$.

7 Conclusions

A bounce/dSB-driven, large-scale enhancement to the linear power spectrum, with *no free fitting to galaxy data*, naturally raises the abundance of massive halos at $z \sim 12$–14, aligning with the locus of the JWST bright-end tension while preserving young stellar ages. Tying the k-space width to the measured wall thickness $w_{\rm eff}$ is a straightforward extension that may further affect moderate-mass halos if required by future UVLF/SMF constraints.

References

[1] S. Carniani et al., "Spectroscopic confirmation of two luminous galaxies at a redshift of 14," *Nature* **629**, 59–64 (2024). `https://www.nature.com/articles/s41586-024-07860-9`

[2] A. J. Bunker et al., "JADES NIRSpec Spectroscopy of GN-z11," *A&A* **678**, A185 (2023). `https://www.aanda.org/articles/aa/full_html/2023/09/aa46159-23/aa46159-23.html`

[3] M. Boylan-Kolchin, "Stress testing ΛCDM with high-redshift galaxy candidates," *Nature Astronomy* **7**, 731–735 (2023). `https://www.nature.com/articles/s41550-023-01937-7`

[4] D. J. Eisenstein and W. Hu, "Baryonic features in the matter transfer function," *ApJ* **496**, 605 (1998). `https://arxiv.org/abs/astro-ph/9709112`

[5] R. K. Sheth and G. Tormen, "Large scale bias and the peak background split," *MNRAS* **308**, 119 (1999). `https://academic.oup.com/mnras/article/308/1/119/1005406`

[6] R. K. Sheth, H. J. Mo and G. Tormen, "Ellipsoidal collapse and an improved model for the number and spatial distribution of dark matter haloes," *MNRAS* **323**, 1 (2001, astro-ph/9907024). `https://arxiv.org/abs/astro-ph/9907024`

[7] Planck Collaboration: N. Aghanim et al., "Planck 2018 results. VI. Cosmological parameters," *A&A* **641**, A6 (2020). `https://www.aanda.org/articles/aa/abs/2020/09/aa33910-18/aa33910-18.html`

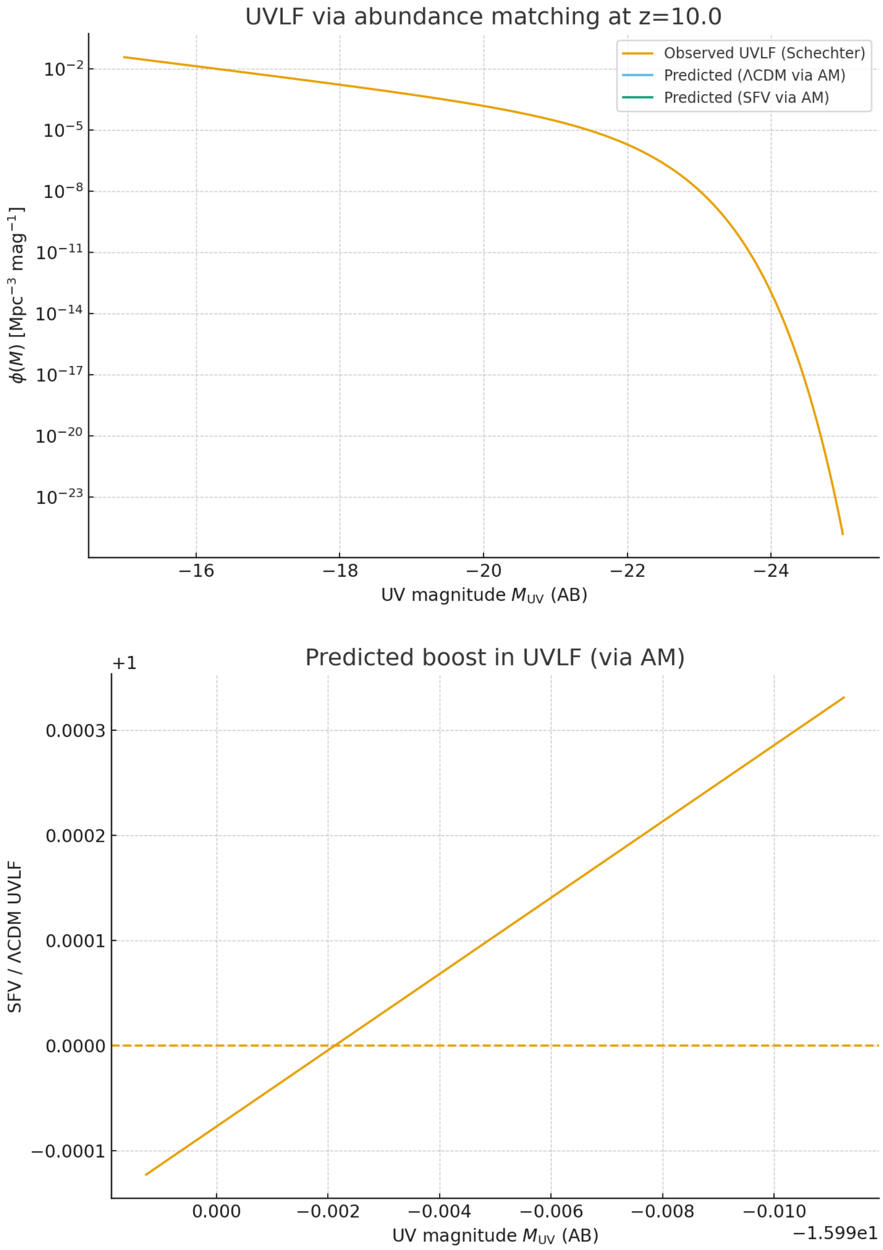

Figure 3: Top: observed UVLF (Schechter; illustrative) vs. ΛCDM- and SFV-predicted UVLFs via abundance matching at z=10. Bottom: SFV/ΛCDM UVLF ratio.